

lengths in the wave functions for the alpha particle in Li^6 , and for the proton in He^3 , respectively; η is defined, approximately, by $\tan\eta = \gamma/Z + 1/Zr_0$.

This result has the same form as the deuteron pickup angular distribution. However, because Z is smaller than the corresponding K , appropriate for deuteron pickup, the oscillations in the backward direction can be fitted only with a much larger radius than for the other process. This is illustrated by curve d in Fig. 4, computed from the relation above, at 18.5 Mev for $r_0 = 8.4 \times 10^{-13}$ cm, with arbitrary normalization. Also, the angular distribution should shift considerably on lowering the proton energy. This is illustrated by curve c , in Fig. 3, calculated for the same radius, at 15 Mev. The impossibly large radius, and the fact that no shift is observed between the angular distributions at the two energies, suggest that the minimum, observed

at 140 degrees, cannot be explained in this simple way. For a reasonable nuclear radius, say 5×10^{-13} cm, the relation above gives an almost isotropic angular distribution from 90 to 180 degrees; lack of isotropy must be due to the angular dependence of the proton-alpha scattering amplitudes. While the minimum at 140 degrees, in Fig. 3, might be related to the minimum observed in proton-alpha scattering,²⁵ a full explanation must await further developments in the theory.

It is a pleasure to thank Professor R. Sherr, Professor P. C. Gugelot, and Professor M. G. White for their interest and advice in this work. We are also indebted to Dr. K. G. Standing, Dr. J. B. Reynolds, and Dr. G. Schrank for valuable comments, and for the use of their equipment.

²⁵ K. W. Brockman, Phys. Rev. **102**, 391 (1956).

Alpha-Alpha Scattering at Low Energies*

N. P. HEYDENBURG AND G. M. TEMMER

Department of Terrestrial Magnetism, Carnegie Institution of Washington, Washington, D. C.

(Received June 13, 1956)

We have measured the differential cross section for the scattering of alpha particles in helium between laboratory angles of 10 and 80 degrees and in the energy range 150 kev to 3 Mev, using He^+ ions from our electrostatic generators. Below 400 kev no nuclear interaction occurs within the accuracy of the experiments ($\pm 1\%$), and Mott's formula for the Coulomb scattering of identical zero-spin particles is verified in detail. Above 400 kev the nuclear s -wave interaction begins to contribute, starting at a phase shift K_0 near π , and smoothly decreasing with increasing energy to about 128 degrees at 3 Mev. Starting at 2.5 Mev, a small d -wave phase shift, K_2 is found necessary to account for the observed angular distributions, reaching a value of 2.5 degrees at 3 Mev. Absolute values of the cross sections were determined by fitting the relative angular distributions with the single parameter K_0 below 2 Mev, and by comparison with Rutherford scattering in argon above 2 Mev. The phase shift analysis was facilitated by a simple mechanical monograph described in Appendix III. A careful survey of the low-energy region containing the ground state of Be^8 , and the absence of any measurable effect leads to a lower limit for the mean life of the ground state of Be^8 of 2×10^{-16} sec. Combined with a recently established upper limit of 4×10^{-16} sec, this locates the lifetime to within a factor of twenty.

I. INTRODUCTION

THE alpha particles from natural emitters in the heavy elements, whose energies lie in the range between 4 and 8 Mev, were the first projectiles to be used in the exploration of the nuclear force field. Rutherford and his co-workers¹ were able to demonstrate deviations from the Coulomb law of force at large scattering angles, thus establishing a rough value for the nuclear radius. During these early measurements the scattering of alpha particles in helium, among many other elements, was investigated

as a function of energy by slowing down natural alpha particles with absorbers. These measurements were necessarily crude because of the extremely low available intensities, and consequent large spreads in energy and angle. Although it was realized that the ordinary Rutherford scattering expression had to be modified because of the impossibility of distinguishing the scattered from the scattering particle, this modification was considered merely a technical necessity. Experiments were not extended to sufficiently low energies to permit the discovery of a fundamental discrepancy. In fact, the ratio of observed cross section to Rutherford cross section, at 45 degrees in the laboratory, happened to pass through unity around 4 Mev, and hence there was no apparent incentive to pursue the investigation to still lower energies, since the interest centered on deviations from Rutherford scattering.

* Preliminary accounts of this work may be found in Cowie, Heydenburg, Temmer, and Little, Phys. Rev. **86**, 593(A) (1952), and G. M. Temmer and N. P. Heydenburg, Phys. Rev. **90**, 340(A) (1953).

¹ For discussion of the earliest work on α - α scattering, see Rutherford, Chadwick, and Ellis, *Radiations from Radioactive Substances* (Cambridge University Press, Cambridge, England, 1930).

Mott² pointed out the fundamental consequences of the quantum-mechanical concept of identity when applied to the Coulomb scattering of identical particles. The first experiment designed to test the rather striking predictions of Mott was carried out by Chadwick³ who was able to show that at very low energies (~ 1 Mev) approximately twice the number of alpha particles were scattered at 45° (lab) than was predicted classically. Blackett and Champion,⁴ from an analysis of cloud chamber photographs further concluded that a deficiency in the scattering did exist at around 25 degrees as predicted by Mott's formula. Later experiments on alpha-helium scattering were performed mainly to determine deviations from Mott scattering, i.e., to study the influence of the specifically nuclear force on the interaction between alpha particles.⁵⁻⁷

A theoretical interpretation of these early measurements up to 1939 was made by Wheeler.⁸ He performed a phase shift analysis for alpha energies up to 7 Mev and concluded that the energy level in Be⁸ located at about 3 Mev (6 Mev scattering) must have spin zero, in contrast to the evidence obtained from most other experiments involving this level which seemed to demand $I=2$. It must be remembered that the experimental errors incurred in these early experiments were rather large and allowed considerable freedom in the choice of phase shifts. More theoretical work, based on the same data, was carried out more recently.⁹

The alpha-helium scattering was continued with cyclotrons after the war at 20 Mev,¹⁰ 32 Mev¹¹, and lately again at 22 Mev¹² and 12 Mev.¹³ Up to four phase shifts had to be invoked for the interpretation of these experiments.

It was apparent that the region of pure s -wave interaction, as well as of the interaction involving only s and d waves was rather unexplored. (It should be remembered that only even angular-momentum waves can participate in the scattering of identical particles of zero spin.) When we were successful in obtaining large beams of singly-charged helium ions from both our electrostatic generators equipped with rf ion sources, we decided to investigate the scattering of alpha particles in helium with three specific objectives in mind: (1) to verify Mott's formula in detail at energies so low that all nuclear effects have disappeared; (2) to explore the region of the ground state of Be⁸ in order to

set an upper limit to its width and hence a lower limit to its lifetime; (3) to determine the s -wave and d -wave phase shifts from their first appearance up to 3 Mev, and possibly to shed some light on the 3-Mev level in Be⁸. We shall discuss these experiments in turn.

II. THEORETICAL BACKGROUND

The ratio of the differential scattering cross section to that expected on the basis of the pure Coulomb interaction of identical, zero-spin particles (Mott scattering) is given by the following expression:

$$\frac{d\sigma(\Theta)}{d\sigma_M(\Theta)} \equiv R(\Theta) = \left| A'(\Theta) + A''(\Theta) + \sum_{\substack{L=0 \\ \text{(even)}}}^{\infty} A_L(\Theta) (e^{2iK_L} - 1) \right|^2, \quad (1a)$$

where

$$A'(\Theta) = \frac{1}{\sqrt{\sigma_M}} \csc^2 \Theta \exp(i\eta \ln \csc^2 \Theta); \quad (1b)$$

$$A''(\Theta) \equiv A'(\frac{1}{2}\pi - \Theta) = \frac{1}{\sqrt{\sigma_M}} \sec^2 \Theta \exp(i\eta \ln \sec^2 \Theta);$$

$$\sigma_M = \csc^4 \Theta + \sec^4 \Theta + 2 \csc^2 \Theta \sec^2 \Theta \times \cos(\eta \ln \tan^2 \Theta); \quad \eta = 4e^2/\hbar v; \quad (1c)$$

$$A_L(\Theta) = \frac{2i}{\eta} \frac{1}{\sqrt{\sigma_M}} (2L+1) P_L(\cos 2\Theta) e^{2i\xi_L}; \quad (1d)$$

$$\xi_L = \sum_{k=1}^L \tan^{-1}(\eta/k); \quad \xi_0 = 0. \quad (1d)$$

Θ is the scattering angle in the laboratory system [$\Theta = \theta/2$, θ = scattering angle in the center-of-mass (c.m.) system]; A' and A'' represent the Coulomb scattering amplitudes for scattered and scattering particles, respectively; the quantities A_L are the specifically nuclear scattering amplitudes for angular momentum L , exclusive of the phase factors, and the sum is extended over all even angular momenta whose partial waves have nonvanishing phase shifts K_L . For energies below 2.0 Mev we find a satisfactory fit of our data using s -wave interaction alone. At the higher energies some d -wave admixture was required. We refer to Appendix I for the explicit expressions for the special cases of pure s wave as well as ($s+d$)-wave scattering.

The ultimate objective of this experiment was of course to fit the experimentally obtained angular distributions at different energies with the expressions given in Appendix I, and thus to obtain values of the phase shifts as a function of the energy. We postpone a description of the mechanics of this determination until later.

² N. F. Mott, Proc. Roy. Soc. (London) **A126**, 259 (1930).

³ J. Chadwick, Proc. Roy. Soc. (London) **A128**, 120 (1930).

⁴ P. M. S. Blackett and F. C. Champion, Proc. Roy. Soc. (London) **A130**, 380 (1931).

⁵ P. Wright, Proc. Roy. Soc. (London) **A137**, 677 (1932).

⁶ C. B. O. Mohr and G. B. Pringle, Proc. Roy. Soc. (London) **A160**, 193 (1937).

⁷ S. Devons, Proc. Roy. Soc. (London) **A172**, 559 (1939).

⁸ J. A. Wheeler, Phys. Rev. **59**, 16 (1941).

⁹ R. R. Haefner, Revs. Modern Phys. **23**, 228 (1951).

¹⁰ K. B. Mather, Phys. Rev. **82**, 126 (1951).

¹¹ E. Graves, Phys. Rev. **84**, 1250 (1951).

¹² F. E. Steigert and M. B. Sampson, Phys. Rev. **92**, 660 (1953).

¹³ Kerman, Nilson, and Jentschke (to be published).

III. EXPERIMENTAL DETAIL

A. Beam

For the work below 1 Mev we used our 1-Mev electrostatic generator. For the energy region between 1 Mev and 3 Mev the scattering apparatus was moved to our pressurized generator. Both of these accelerators are equipped with radio-frequency ion sources of the type described in the literature.¹⁴ The beam of singly-charged helium ions is collimated by two circular apertures of 1 mm diameter separated by a distance of about 80 cm. In addition, a series of some 200 aluminum diaphragms 0.001 in. thick with 2-mm diameter holes, and separated by slightly larger spacers, fill one of the differential pumping canals for a total distance of about 10 cm, thus making energy degradation of the beam by small angle scattering from the canal walls very improbable. Two stages of differential pumping separate the main vacuum from the scattering chamber, where the scattering-gas pressure never exceeded 2.5 mm Hg at the higher energies, and was kept around 0.5 mm Hg below 1 Mev. This corresponds to an effective target thickness, as seen by the movable counter, of less than 50 ev. The beam current in the scattering chamber was of the order of a few microamperes.

B. Scattering Apparatus

The scattering chamber contains a movable proportional counter which may be set accurately to within one minute of arc on either side of the beam, as well as two fixed monitor counters at about 15 degrees. The slit system on the movable counter defines both the scattering volume and the solid angle. The mean angle subtended in the plane of the counter is about one degree. A reentrant charcoal trap immersed in liquid air is attached to the chamber to remove impurities accumulating during a run. The helium scattering gas is fed to the chamber through another charcoal trap. An independent helium supply is used for filling the counters to a pressure of about 5 cm Hg. Because of the high beam intensity it was possible to have a very small aperture in the movable counter (0.5 mm diam). We were thus able to use extremely thin, unsupported Formvar windows ($\sim 5\text{--}10 \mu\text{g}/\text{cm}^2$) which permitted us to detect alpha particles down to 30 kev. The collection voltage for the proportional counters was about 300 volts (when using helium) and was supplied by dry cells.

The output pulses from the proportional counters were fed through conventional preamplifiers, linear amplifiers and scalars. The scalar discriminators for the two monitors were set on the plateau of the counting rate *vs* integral bias curves. The output from the movable scattering counter was simultaneously fed to three scalars with judiciously chosen discriminator settings to insure proper detection efficiency at all

energies covered in an angular distribution measurement, as well as to keep a continuous check on the larger pulses due to scattering from (heavier) impurities. The introduction of the slit system described above vastly improved the plateau characteristics observed in the pulse-height distributions.

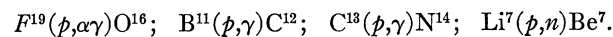
D. Beam Current Measurements

For energies below 1.5 Mev it was found to be impossible to integrate the beam current by the conventional Faraday cup technique because of the large energy loss and excessive scattering of the beam in the thinnest available nickel foil (0.00002 in.). We therefore measured angular distributions relative to the 15° monitors. Since only a single phase shift turned out to be important in this energy range, there was no ambiguity as to the absolute value of the scattering cross sections since the latter is uniquely determined once the *s* phase is found from the angular distribution. [See Eq. (A.1).]

Above 1.5 Mev we used a Faraday cup with nickel foil (see above) and obtained our absolute normalization by scattering from argon. Because of the different charge states of the helium beam (He^0 , He^+ , He^{++}) after emerging from the foil, the actual current collected is a rather complicated function of the number of particles. In fact, Fig. 8 (Appendix III) shows the cross section (multiplied by E^2) for scattering from argon as a function of the energy. The plateau value reflects the predominance of He^{++} ions in the Faraday cup at the higher energies; as we go down in energy, the *apparent* cross section increases because of the smaller average charge per particle collected. Some conclusions on the charge states of the helium ions emerging from the nickel foil are presented in Appendix II. The scattering at each energy was compared to argon scattering for the same nickel foil, and hence an absolute value could be obtained. Current values were used only for the relative comparison of the scattering for the two gases at the same energy. The pure Rutherford behavior for argon was established both from the plateau seen in Fig. 8 (proving the $1/E^2$ dependence of the cross section), and from the exact $\text{csc}^4(\theta/2)$ dependence out to 45 degrees (lab). All usual precautions were taken concerning the proper operation of the Faraday cup such as guard ring, bias voltage, and magnetic field to minimize secondary-emission effects.

D. Energy Calibrations

The energy of the electrostatic generators was calibrated by known gamma-ray resonances and neutron thresholds¹⁵ in the following reactions:



Care was taken to operate the rf ion source at the same

¹⁴ Moak, Reese, and Good, *Nucleonics* 9, 18 (1951).

¹⁵ F. Ajzenberg and T. Lauritsen, *Revs. Modern Phys.* 27, 77 (1955).

probe potential (about 800 volts) during the calibration runs and the actual experiments.

E. Procedure

Below 1.5 Mev, we determined the ratios of counting rates in the movable counter to the counting rate in the monitor on the opposite side of the beam. These measurements were taken for the same angle on both sides of the beam, interspersed by determinations of the ratio of counting rates in the two monitors. The later served as a sensitive indicator of beam position. This set of readings made it possible to obtain a proper average value for a given scattering angle. We covered the range of scattering angles from 10 degrees up to the largest possible angle permitting 100% detection efficiency, in five-degree steps. The maximum angle varied from 50 degrees at the lowest energies to 80 degrees at 3 Mev. Additional angles were chosen for theoretical reasons [e.g., vanishing of $P_2(\cos 2\Theta)$] when needed.

Above 1.5 Mev, where we used the Faraday cup, we took readings on both sides of the beam and again determined average values for all angles. Only one reading with argon gas in the chamber was then necessary at each energy to obtain our absolute cross-section values at all angles, since we had previously established the $\csc^4(\theta/2)$ variation with angle for argon.

The gas pressure in the scattering chamber was read to 0.1% on a butyl phthalate manometer before and after each count in the "Faraday cup" energy region. The gas temperature was found to remain constant to within better than 1°C. In the "monitor counter" energy region these factors did of course not affect the results.

We collected about 10 000 counts at each angle, so that the statistical error was of the order of 1%.

The extent of the contribution of impurities in the scattering gas was determined once during each complete run by setting the counter at a large enough angle ($\Theta \geq 75^\circ$) so that proportional counter pulses due to alpha particles scattered by helium could easily be distinguished from those scattered by the heavier impurities (carbon, nitrogen, oxygen, argon, etc.) by their pulse heights. The contribution at smaller angles could then be calculated from the $\csc^4(\theta/2)$ law. After the introduction of the liquid air-charcoal trap, this contribution was kept below 0.5% for the smallest scattering angle.

A very useful property of the scattering of identical particles is the symmetry of the cross section about 90° (c.m.) or 45° in the laboratory (after division by $\cos\Theta$). All systematic errors but one will show up as a lack of symmetry about 45° (lab). As can be seen from our curves in Fig. 4, symmetry prevails within about 2% for all determinations. This fact confirms (1) the correctness of the $\sin\Theta$ effective target thickness modification, characteristic of gas scattering experi-

ments, (2) the smallness of impurity contributions, (3) the absence of sizable effects due to multiple scattering in the gas (the last two tend to raise the left half of the curves with respect to the right), and (4) the essential correctness of beam and counter alignment. The one possible systematic error which would not give rise to asymmetry is the presence of low-energy components in the incident beam due to degradation by scattering from slits or differential pumping canals. Even a small contamination of this kind is serious because it is weighted as $1/E^2$. We believe that the construction of our collimating slits, described in Sec. III A, minimized this possibility, a belief that is supported by the flat integral pulse-height distribution observed for the scattered particles, as well as by the excellent agreement with Mott scattering at the very low energies where this effect would be most important.

IV. RESULTS

A. General

Our results consist of a number of angular distributions obtained with alpha particles having energies between 150 kev and 3 Mev. Absolute values at 1 Mev and below have been assigned by normalizing the experimental angular distributions for the best-fitting theoretical *s*-wave distributions [see Eq. (A.1), Appendix I], and by comparison with scattering from argon (see above) at 1.5 Mev and above. Our experimental results are summarized in Table I where we list the absolute differential cross sections both in the center-of-mass system and in the laboratory system, as well as the "ratio to Mott" values. The Mott cross section in the c.m. system is given by

$$\left(\frac{d\sigma_M}{d\Omega}\right)_{\text{c.m.}} = \frac{0.0830}{E_0^2} [\csc^4\Theta + \sec^4\Theta + 2 \csc^2\Theta \sec^2\Theta \cos(\eta \ln \tan^2\Theta)] \text{ barns}, \quad (2)$$

where E_0 is the lab energy in Mev. The relation between c.m. and lab cross sections is given by

$$(d\sigma/d\Omega)_{\text{lab}} = 4 \cos\Theta (d\sigma/d\Omega)_{\text{c.m.}} \quad (3)$$

A summary plot of all angular distribution data in terms of the ratio to Mott scattering is given in Fig. 1, where the solid curves represent the best *theoretical* fits we obtain from a phase-shift analysis to be described in Appendix III. These phase shifts are tabulated in Table II. Figure 2 shows a plot of the phase shifts K_0 and K_2 as a function of the energy.

In Fig. 3 we have replotted some of our higher energy data at *constant* angle as a function of the energy to facilitate comparison with the data of the early workers.^{3,5-7} It may be seen that our results tie in fairly well with the older work where overlap exists, in fact surprisingly well in view of the crudeness of the early measurements. It should be recalled that existing

TABLE I. Summary of differential cross sections for alpha-alpha scattering at low energies. Θ =scattering angle in the laboratory system; θ =scattering angle in the cm system; σ_{lab} and $\sigma_{\text{c.m.}}$ are differential cross sections in barns/steradian; R =ratio of observed to Mott scattering [see Eq. (1).] Uncertainties shown are somewhat larger than the purely statistical errors to include variations of successive determinations. σ_{lab} and $\sigma_{\text{c.m.}}$ have same percent errors as R .

Θ	θ	$E_{\text{lab}}=0.600$ Mev			$E_{\text{lab}}=0.850$ Mev			$E_{\text{lab}}=1.00$ Mev		
		σ_{lab}	$\sigma_{\text{c.m.}}$	R	σ_{lab}	$\sigma_{\text{c.m.}}$	R	σ_{lab}	$\sigma_{\text{c.m.}}$	R
15	30	187.4	48.5	1.00±0.01	85.0	22.0	0.98±0.01	57.4	14.9	0.930±0.01
20	40	47.6	12.7	0.99±0.01	22.4	5.97	0.92±0.01	15.8	4.20	0.868±0.01
25	50	18.2	5.00	0.98±0.01	10.4	2.74	0.91±0.01	7.73	2.13	0.913±0.01
30	60	12.2	3.52	0.98±0.01	7.23	2.09	0.98±0.01	6.54	1.63	0.992±0.01
35	70	11.4	3.47	1.00±0.01	6.49	1.98	1.04±0.01	5.07	1.55	1.09 ±0.01
40	80	11.4	3.70	1.02±0.01	6.03	1.97	1.07±0.01	4.70	1.53	1.14 ±0.01
45	90	10.8	3.81	1.03±0.01	5.61	1.98	1.08±0.01	4.32	1.53	1.15 ±0.01
50	100	9.35	3.63	1.00±0.01	5.12	1.99	1.08±0.01	3.91	1.52	1.13 ±0.01
55	110	7.90	3.45	0.99±0.01	4.61	2.01	1.06±0.01	3.55	1.55	1.09 ±0.01
60	120	7.01	3.51	0.98±0.01	4.18	2.09	0.98±0.01	3.31	1.66	1.01 ±0.02
65	130	8.26	4.88	0.96±0.01	4.74	2.81	0.93±0.01
70	140	16.6	12.1	0.95±0.01	8.19	5.99	0.92±0.01
75	150	48.6	46.9	0.97±0.01	22.9	22.1	0.98±0.01

Θ	θ	$E_{\text{lab}}=1.50$ Mev			$E_{\text{lab}}=2.00$ Mev			$E_{\text{lab}}=2.50$ Mev			$E_{\text{lab}}=3.00$ Mev		
		σ_{lab}	$\sigma_{\text{c.m.}}$	R	σ_{lab}	$\sigma_{\text{c.m.}}$	R	σ_{lab}	$\sigma_{\text{c.m.}}$	R	σ_{lab}	$\sigma_{\text{c.m.}}$	R
10	20	138.5	35.14	0.89±0.01	65.8	16.73	0.78 ±0.01	28.0	7.11	0.74 ±0.01
15	30	22.5	5.83	0.81±0.01	11.19	2.90	0.69 ±0.01	6.03	1.56	0.565±0.01	3.61	0.933	0.475±0.01
20	40	6.84	1.82	0.76±0.01	3.71	0.986	0.68 ±0.01	2.18	0.579	0.593±0.01	1.40	0.373	0.530±0.01
25	50	3.83	1.05	0.87±0.01	2.40	0.664	0.89 ±0.01	1.65	0.455	0.912±0.02	1.21	0.332	0.93 ±0.02
27°22'	54°44'	3.39	0.953	0.97±0.01	2.22	0.625	1.05 ±0.02	1.61	0.403	1.14 ±0.02	1.16	0.328	1.15 ±0.02
30	60	3.11	0.898	1.09±0.02	2.13	0.617	1.25 ±0.02	1.56	0.451	1.38 ±0.02	1.17	0.337	1.45 ±0.02
35	70	2.80	0.852	1.27±0.02	1.96	0.601	1.54 ±0.02	1.48	0.451	1.78 ±0.03	1.10	0.335	1.88 ±0.03
40	80	2.63	0.857	1.41±0.02	1.85	0.605	1.75 ±0.03	1.37	0.427	2.01 ±0.03	1.01	0.330	2.14 ±0.03
45	90	2.42	0.856	1.45±0.02	1.69	0.599	1.80 ±0.03	1.27	0.448	2.11 ±0.03	0.927	0.328	2.22 ±0.03
50	100	1.69	0.838	1.38±0.02	1.54	0.598	1.73 ±0.03	0.866	0.336	2.18 ±0.03
55	110	2.01	0.879	1.31±0.02	1.57	0.620	1.59 ±0.02	0.785	0.342	1.92 ±0.03
60	120	1.83	0.914	1.11±0.02	1.23	0.617	1.25 ±0.02	0.721	0.361	1.55 ±0.03
65	130	1.82	1.08	0.89±0.02	1.14	0.676	0.91 ±0.02	0.558	0.330	0.92 ±0.02
70	140	2.50	1.83	0.76±0.02	1.35	0.994	0.68 ±0.02	0.510	0.373	0.530±0.02
75	150	6.33	6.11	0.85±0.02	2.96	2.87	0.68 ±0.02	0.989	0.955	0.486±0.02
80	160	22.2	32.0	0.81±0.02	7.16	10.33	0.481±0.03	4.94	7.11	0.74 ±0.03

theoretical interpretations^{8,9} of alpha-alpha scattering have had to work within the large margins of error of natural emitter data. Consequently, the theoretical "fits" often fall quite wide of the mark set by our more accurate data. It is therefore not too surprising that apparent contradictions exist in the phase-shift analysis of the alpha-alpha scattering and spin assignments of excited states in Be⁸. Recently a group at the Rice Institute¹⁶ has extended these measurements from 3-Mev to 6-Mev bombarding energy; their results are in excellent agreement with ours at the 3-Mev point of overlap.

We detected definite deviations from Mott scattering at 600 kev and above (see Fig. 2 above). However, no nuclear effects were found at 400 kev and below within our experimental error ($\pm 1.5\%$). Figure 4 shows our results for the lowest energy at which we measured an angular distribution (150 kev). The absolute differential scattering cross section in the center-of-mass system is shown, normalized to the theoretical Mott curve at 40° (c.m.). The very pronounced interference effects due to particle identity are in evidence and agree perfectly with the predicted Mott formula. Two maxima

and two minima may be discerned. It should be noted that the interference term at this low energy is extremely energy sensitive because of the large value of η , and hence of the argument of the cosine term in Eq. (1c). A 5-kev shift in the theoretical curve will produce appreciable discrepancies with experiment. The agreement increases our confidence in the essential correctness of the energy scale in this region.

It is interesting to note that comparably strong interference effects in proton-proton scattering, i.e., similar values for η [Eq. (1c)] would have to be sought at proton energies of one sixty-fourth the corresponding alpha-particle energy, or around 2 kev in our example.

TABLE II. Summary of s - and d -wave phase shifts for low-energy alpha-alpha scattering. Incident energy in Mev; phase shifts in degrees.

E_{lab}	K_0	K_2
0.400	0 ±0.5	0
0.600	178 ±1	0
0.850	175 ±1	0
0.950	173 ±1	0
1.00	171 ±1	0
1.50	159 ±1	0
2.00	148 ±1	0.0±0.1
2.50	137.5±1	1.0±0.2
3.00	128.4±1	2.5±0.3

¹⁶ Phillips, Russell, and Reich, Phys. Rev. **100**, 960 (1956); also Russell, Phillips, and Reich, Phys. Rev. **104**, 135 (1956), following paper.

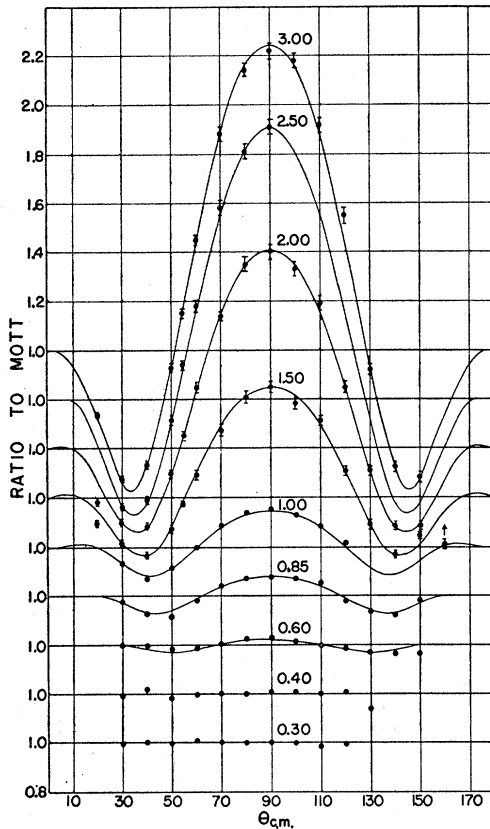


FIG. 1. Summary of angular distributions for α - α scattering in the energy range 300 kev to 3.00 Mev. Ratio of observed to Mott differential cross sections is plotted against center-of-mass scattering angle θ . Values at center of curves refer to bombarding energy in Mev. Vertical scale shown correctly for the highest curve (3 Mev), but arbitrarily displaced by 0.20 unit downward for 2.5 Mev, 0.40 unit for 2.0 Mev, etc., to avoid superposition. The value 1.0 belonging to each energy is indicated to the left. Curves, symmetrical about 90° , are *theoretical*, obtained by phase-shift analysis of the data, using the values for s -wave and d -wave phase shifts K_0 and K_2 listed in Table II. No nuclear effect observed at 300 and 400 kev; K_0 alone accounts for distributions from 600 kev to 2 Mev, while both K_0 and K_2 are required to fit 2.5 and 3.0 Mev. Data for 150 kev, 200 kev, and 950 kev are not shown. Errors indicated combine statistical uncertainty and internal consistency of various runs. Some low points at large angles are due to fall-off in detection efficiency for scattered alpha particles having energies below ~ 40 kev.

B. Ground State of Be^8

Figure 5 shows the results of a careful survey of the energy region containing the ground state of Be^8 , whose energy is reported at 94.5 ± 1.4 kev from the Q value of the $\text{Be}^8(p,d)\text{Be}^8$ reaction.¹⁷ Measurements were obtained every 500 ev (and in part every 250 ev) at a fixed scattering angle of $\Theta = 45^\circ$. The curve shows the ratio of scattering to monitor counts as a function of incident alpha-particle energy. The slight slope in the curve is exactly accounted for by the velocity dependence of the Mott interference term at $\Theta = 15^\circ$

¹⁷ Jones, Donahue, McEllistrem, Douglas and Richards, Phys. Rev. **91**, 879 (1953).

[location of monitor counter, see Eq. (1c)]; there is no energy dependence (other than $1/E^2$) at $\Theta = 45^\circ$, as can be seen from Eq. (1c). We find no deviation outside our experimental error ($\sim 2\%$) from pure Mott scattering over the entire region investigated, namely 146 kev to 202 kev (lab), or 73 kev to 101 kev (c.m.). This observation has the following significance: Figure 6 shows the theoretically expected scattering anomaly in the quantity $R_0(45^\circ)/R_0(15^\circ)$, where $R_0(\Theta)$ is given by Eq. (A.1) of Appendix I, over a phase-shift interval of π in the s -wave component, since Be^8 has a ground-state spin $I=0$.¹⁸ The phase shift as a function of the energy must be purely of the resonant type, and is given by the expression

$$K_0 = \tan^{-1} \left(\frac{\frac{1}{2}\Gamma}{E_r - E} \right), \quad (4)$$

where E_r and E represent the resonance energy and the alpha-particle energy, respectively, and Γ is the full width at half maximum of the Be^8 ground state, all expressed in the laboratory system. We are certainly justified in neglecting any nuclear *potential* phase shift contributions at these energies, since we still observe only pure Mott scattering at energies as high as 400

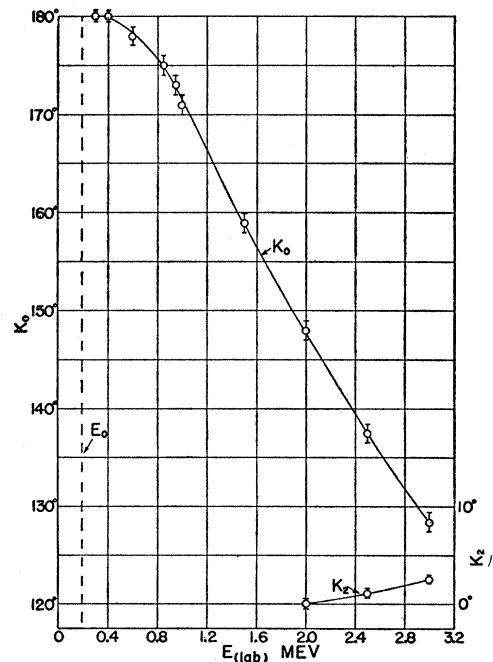


FIG. 2. Dependence of phase shifts for α - α scattering on energy. Left-hand scale applies to s -wave phase shift K_0 ; right-hand scale applies to d -wave phase shift K_2 . Errors shown are determined from the uncertainties in the angular distribution data as illustrated in Fig. 10. Dotted vertical line marked E_0 at 189 kev represents probable behavior of K_0 upon going through the resonance corresponding to the ground state of Be^8 . [See Fig. 6 and Sec. IV (b).]

¹⁸ P. B. Treacy, Proc. Phys. Soc. (London) **A68**, 204 (1955).

kev. Now the resonance corresponding to the ground state is bound to be very narrow compared to the inherent stability and energy spread of our alpha-particle beam. We must therefore evaluate the effect of a narrow anomaly of the type shown in Fig. 6 on a beam whose natural spread ΔE is estimated to be about 250 ev.¹⁹ We relegate to Appendix IV a more detailed evaluation of this problem, and merely state the result obtained for the *upper limit* on the level width:

$$\Gamma_0 \leq 3.5 \text{ ev,}$$

based on the absence of any observable effect greater than 2%. This implies a *lower limit* on the mean life τ of the ground state of Be⁸ given by

$$\tau \geq \frac{\hbar}{\Gamma_0} = \frac{6.64 \times 10^{-16}}{\Gamma_0(\text{ev})} = 2 \times 10^{-16} \text{ sec.}$$

It is interesting to note that there exist a number of *upper* bounds on the lifetime of this state, deduced from cosmic-ray star fragments.^{20,21} From the fact that Be⁸ fragments break up into two alpha particles within less than 0.5 micron (lower limit of resolution in emulsion) of the origin of an energetic event ("star"), Hodgson sets an *upper* limit on τ of

$$\tau \leq 2 \times 10^{-14} \text{ sec.}$$

More recently, Treacy,¹⁸ from a study of the B¹¹(p,α)Be⁸ reaction, inferred an *upper* limit

$$\tau \leq 4 \times 10^{-15} \text{ sec.}$$

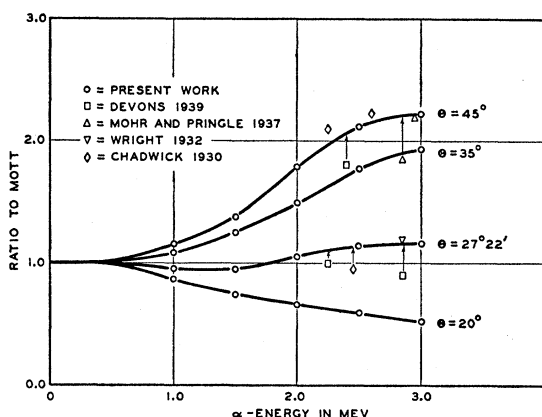


FIG. 3. Summary of data on α - α scattering at fixed scattering angles vs energy. Ratio to Mott of observed differential cross sections at $\Theta=20^\circ$, $27^\circ 22'$, 35° , and 45° (lab). Early data, obtained exclusively with natural alpha emitters, usually refer to angular spread of $\sim 10^\circ$ about the nominal angles, and have large uncertainties in their energy values. For early data, see references 3, 5, 6, and 7.

¹⁹ This spread is composed of about 200 volts due to the 0.1% voltage regulation of the generator, the rest being ascribed to the small gas target thickness, and the inherent uncertainty in knowing the exact potential at the place of ion formation in the rf ion source.

²⁰ J. Crussard, Compt. rend. 231, 141 (1950).

²¹ P. E. Hodgson, Phil. Mag. 43, 190 (1952).

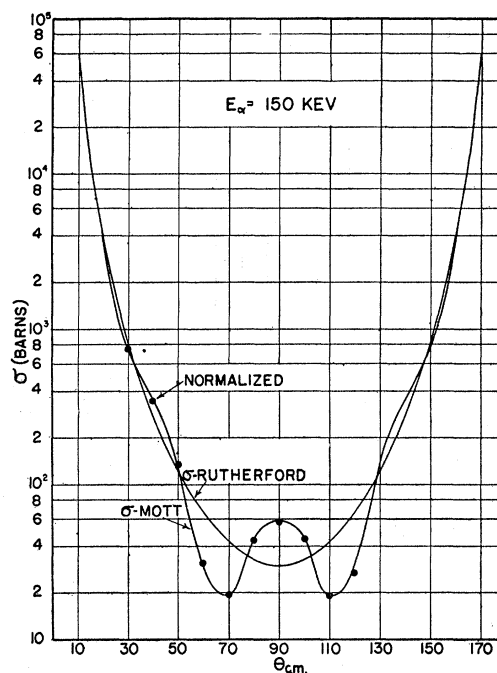


FIG. 4. Angular distribution of α - α scattering at 150 kev, our lowest energy. Data are normalized at 40° to the theoretical Mott curve. Differential cross section in the c.m. system in barns. Rutherford cross section is also shown (no interference term). This represents the most detailed confirmation of the influence of identity on scattering.

The lifetime of the ground state of Be⁸ is therefore bracketed to within a factor twenty as follows:

$$2 \times 10^{-16} \text{ sec} \leq \tau \leq 4 \times 10^{-15} \text{ sec.}$$

C. Corrections

The major correction applied to our scattering data is the well-known "second-derivative" correction to take into account the finite aperture of the counters.²²

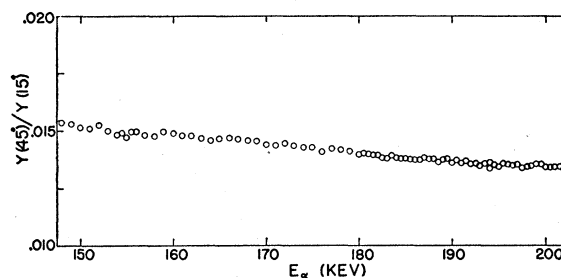


FIG. 5. Search for the ground state of Be⁸. Data represent ratio of scattering at 45° to scattering at 15° (monitor counter) over the energy interval 146 kev to 202 kev. Readings every 250 ev from 180 kev on. Resonance expected at $2 \times 94.5 \text{ kev} = 189 \text{ kev}$ (see reference 17). Scattering is of pure Mott type; slight slope is accounted for by the energy dependence of the interference term in Eq. (1c) for 15° scattering. Each point represents at least 12 000 counts. For conclusions from less than 2% deviation from a straight line, see Appendix IV.

²² Breit, Thaxton, and Eisenbud, Phys. Rev. 55, 1018 (1939).

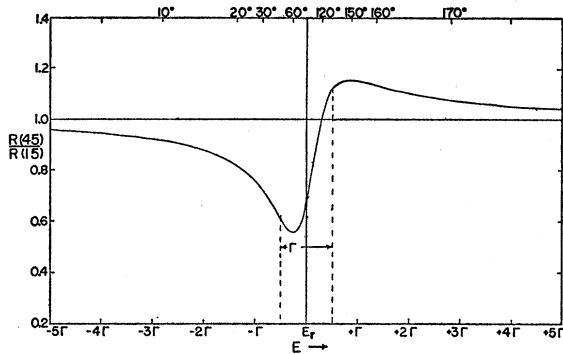


FIG. 6. Theoretical shape for s -wave resonance corresponding to Be^8 ground state. Ratio to the Mott differential cross section at 45° divided by the corresponding ratio at 15° is plotted vs alpha energy, in units of Γ , the full width (lab) of the presumed resonance. Upper abscissa gives corresponding values of K_0 running from 0 to π . For analytic expressions relating these quantities, see Eq. (4) and (A.1).

This amounts to -3.5% at the smallest angle ($\Theta = 10^\circ$) and becomes less than 0.5% for angles greater than 20° . It again reaches 1.3% at $\Theta = 80^\circ$.

The effect of impurities heavier than helium was kept to a minimum by a liquid air—charcoal trap, as has already been mentioned; at no time did the contribution at the smallest angles exceed 0.5% . This could be accurately determined from the pulse-height distribution at large scattering angles, where the energy of alpha particles scattered from helium is $E_0 \cos^2 \Theta$, while it is much nearer E_0 for scattering from impurities such as N_2 or O_2 . Assuming $Z=8$ for a representative impurity, an upper limit of 0.03% can be tolerated to produce a scattering contribution of 0.5% at $\Theta = 15^\circ$.

A number of other corrections, such as multiple Coulomb or nuclear scattering in the gas, the lack of complete parallelism of the beam, etc., were found to be negligibly small.

Because of the extremely steep dependence of the scattering yield on scattering angle,²³ amounting to as much as a change of 0.8% per minute of arc at $\Theta = 10^\circ$, very accurate alignment of the chamber with respect to the beam axis could be achieved from small-angle scattering observations on either side of the beam. Furthermore, all our data were obtained by averaging left and right observations. We estimate that an additional uncertainty of about 1% exists for observations at 10° and 15° . However, from the symmetry of the scattering curves about $\theta = 90^\circ$, small-angle difficulties seem to have been under control.

V. DISCUSSION

A. Region of Pure Coulomb Interaction

Our low-energy data on alpha-helium scattering probably represent the most detailed confirmation of

²³ The cross-section variation is enhanced by the $\csc \Theta$ variation characteristic of gas scattering experiments (effective target thickness).

the consequences of particle identity on scattering as predicted by Mott. The agreement with theory is excellent over the entire interval from 150 keV to about 500 keV, where the first evidence for nuclear s -wave interaction becomes apparent. Our search for the ground state of Be^8 with negative results permits us to set a good *lower* limit on the lifetime of that state which, when combined with upper limits from other experiments, narrows the gap considerably. Bethe made an early estimate of the lifetime of Be^8 based on barrier penetration considerations.²⁴ His estimates for $E_r = 100$ keV (close to the accepted value of 94.5 keV) and for two assumed interaction radii of two alpha particles are given in Table III, together with a summary of the state of affairs for the Be^8 ground state. We also list the *lower* limit for the Be^8 ground state lifetime of spin zero calculated from the sum rule given by Teichmann and Wigner,²⁵ which is about one-fifth of our experimental lower limit. We see that the theoretical estimates certainly encompass the experimental situation.

B. Region of Pure S-Wave Interaction

As can be seen from either Fig. 1 or Fig. 2, the first indication of a need for an s -wave phase shift K_0 occurs at 600 keV. The phase shift is either small and negative, or slightly less than π (see Appendix I). We prefer the latter interpretation in view of the fact that the (nonobserved) resonance in the s wave, corresponding to the ground state of Be^8 , must have caused a phase change of π , so that the s -wave phase could then have started at 0° as indicated by the dotted line in Fig. 2. The s -wave phase shift continues smoothly into the region of 3 MeV to 6 MeV.¹⁶ For a discussion of this behavior in terms of effective-range theory, we refer to the forthcoming publication of the Rice group.¹⁶ The general behavior of the s -wave and d -wave components is just as expected on the basis of a simple alpha-alpha potential such as the one put forward by Haefner⁹ which we show in Fig. 7. Its analytic expression is shown in the figure. Wheeler's earlier interpretation of alpha-alpha scattering experiments⁸ was handicapped by the poor accuracy of early work, which forced him to conclude that the first excited state of Be^8 at about 3 MeV had spin zero, and hence

TABLE III. Lifetime of the ground state of Be^8 . $E_0 = 94.5 \pm 1.4$ keV^a; $I = 0$ ^b; r_0 in units of 10^{-13} cm; τ is the mean life in seconds.

	Theory		Sum rule	Experiment	
	Penetrability $r_0 = 2.5$	$r_0 = 5.0$		$\text{He}^4(\alpha, \alpha)\text{He}^4$	$\text{B}^{11}(\beta, \alpha)\text{-Be}^8(\alpha)\text{He}^4$
τ	3×10^{-16}	4×10^{-17}	$> 4 \times 10^{-17}$	$> 2 \times 10^{-16}$	$< 4 \times 10^{-16}$
Reference	(24)	(25)	(25)	present work	(18)

^a Reference 17.

^b Reference 18.

²⁴ H. A. Bethe, Revs. Modern Phys. **9**, 167 (1937).

²⁵ T. Teichmann and E. P. Wigner, Phys. Rev. **87**, 123 (1952).

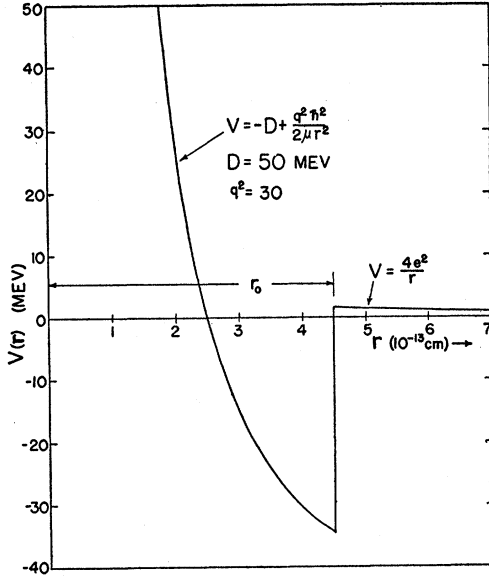


FIG. 7. α - α interaction potential of the type used by Haefner (reference 9). Pure Coulomb potential outside r_0 ; region of attraction inside r_0 , followed by strong repulsion at small distances. r is the distance between centers of alpha particles. Values of $D=50$ Mev and $r_0=4.5 \times 10^{-13}$ cm are arbitrarily chosen here merely for purposes of illustration.

would have to show resonant behavior in the s -wave. He concluded correctly that no static interaction potential could account for such a state.

We found satisfactory fits for pure s -wave interaction at all energies from 600 kev to 2 Mev.

C. Region of d -Wave Interaction

The first definite need for a small amount of d -wave component arises at 2.5 Mev ($K_2=1.0^\circ$, see Appendix III). The work at the Rice Institute¹⁶ definitely showed the d -wave resonance associated with the first-excited state of Be^8 at ~ 3 Mev, thus establishing the spin of the latter as 2^+ . This is as expected for almost any postulated alpha-alpha interaction. We merely observe the onset of the K_2 contribution (see Fig. 2), which amounts to 2.5° at our highest energy; without the benefit of the broad resonance at about 6 Mev (lab), the d -wave due to purely potential scattering would not be expected to contribute until somewhat higher energies are reached.

The $L=4$ partial wave did not have to be considered here; in fact it is not even found to contribute in the Rice work up to 6 Mev, and is detected only in the scattering at 12 Mev and above.^{12,13}

Hence, although the alpha particle is a complex structure in itself, it is found that a relatively simple potential can account in a rather satisfactory manner for all low-energy features of the alpha-alpha interaction. This fact is of special importance for calculations

using the alpha-particle model, such as have recently received renewed attention.²⁶

VI. ACKNOWLEDGMENTS

We thank D. B. Cowie and C. A. Little, Jr., for their contributions to the beginning phases of this work.

APPENDIX I. EXPLICIT EXPRESSIONS FOR LOW-ENERGY α - α SCATTERING

(1) s wave only.—We use Eq. (1) for $L=0$; the summation then consists of a single term involving K_0 . The nuclear amplitude $A_0=2i/\eta\sqrt{\sigma_M}$, where σ_M and η were defined in Eq. (1c). Squaring expression (1a) in this case, we obtain

$$\frac{d\sigma_0(\Theta)}{d\sigma_M(\Theta)} \equiv R_0(\Theta) = 1 + \frac{1}{\sigma_M} \int_0^8 -\sin^2 K_0 \times \left(\frac{2}{\eta} - \csc^2 \Theta \sin \alpha - \sec^2 \Theta \sin \beta \right) - \frac{4}{\eta} \sin 2K_0 (\csc^2 \Theta \cos \alpha + \sec^2 \Theta \cos \beta) \Big], \quad (\text{A.1})$$

where

$$\alpha = \eta \ln \csc^2 \Theta; \quad \beta = \eta \ln \sec^2 \Theta. \quad (\text{A.2})$$

We see that adding π to the phase shift K_0 leaves expression (A.1) unchanged; changing the sign of K_0 , however, changes the sign of the last term in (A.1). All our angular distribution data up to and including 2 Mev could be fitted in a satisfactory way with a single parameter K_0 ; it is clear that the *absolute* differential cross sections in these cases are also determined by K_0 . The values for K_0 listed in Table II for energies up to 2 Mev were obtained from the angular distributions; in addition, the phase shifts at 1.5 and 2 Mev were determined independently from the absolute values obtained by comparison with argon scattering [see Sec. IV(a)], and were found to be in good agreement with the former values.

(2) s wave and d wave only.—For completeness, we list the explicit expression for the scattering involving $L=0$ and $L=2$. The summation in Eq. (1a) extends over two terms now. It is convenient to write $R_2(\Theta)$ in terms of $R_0(\Theta)$, defined in (A.1) above, as follows:

$$\frac{d\sigma_2(\Theta)}{d\sigma_M(\Theta)} \equiv R_2(\Theta) = R_0(\Theta) + \frac{400P_2^2(\cos 2\Theta) \sin^2 K_2}{\eta^2 \sigma_M} - \frac{40}{\eta \sqrt{\sigma_M}} P_2(\cos 2\Theta) (\sin K_2) (\sqrt{R_0}) \times \cos[\psi - (2\xi_2 + K_2)], \quad (\text{A.3})$$

where

$$\xi_2 = \tan^{-1} \eta + \tan^{-1}(\eta/2) \quad (\text{A.4})$$

²⁶ D. M. Dennison, Phys. Rev. 96, 378 (1954).

as defined in (1e), and

$$\psi = \tan^{-1} \left(\frac{\csc^2 \Theta \sin \alpha + \sec^2 \Theta \sin \beta - (4/\eta) \sin^2 K_0}{\csc^2 \Theta \cos \alpha + \sec^2 \Theta \cos \beta - (2/\eta) \sin 2K_0} \right); \quad (\text{A.5})$$

all other symbols have been defined previously. Since two parameters, K_0 and K_2 , are now required to fit a given angular distribution, we have found it preferable to determine them from the experimental data by means of a vectorial nomograph, to be described in Appendix III.

APPENDIX II. CHARGE STATES OF THE HELIUM BEAM

The problem of the fractions of the helium beam being in the respective charge states He^0 , He^+ , and He^{++} is of importance in connection with the determination of our absolute cross sections. As we pointed out in Sec. III(c) above, we used a Faraday cup for scattering at 1.5 Mev and above, using argon scattering of established Rutherford behavior as a calibration, so that we could obtain absolute cross sections by comparison at any given energy, and using the *same* nickel window separating the scattering gas volume from the high vacuum region of the Faraday cup. Fortunately we do not observe any *d*-wave effects until we reach 2.5 Mev (see Fig. 2) so that we are able to get absolute cross sections at the lower energies, where the charge state problem and the problem of scattering in the thin Ni window (0.00002 in. thick) become very serious, from relative angular distributions using monitor counters, as described in Appendix I. Figure 8 illustrates the situation for the higher energies; we plot the reduced yield of alpha particles scattered from argon at $\Theta = 20^\circ$ vs bombarding energy. The reduced yield is given by

$$Y_r = Y E_0^2 / N p, \quad (\text{A.6})$$

where Y is the actual observed yield, N is the number of alphas per unit of charge collected, E_0^2 removes the

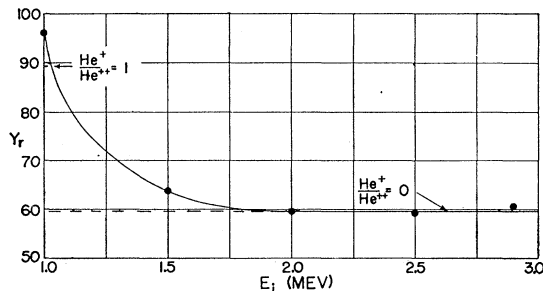


FIG. 8. Reduced yield of alpha particles scattered at $\Theta = 20^\circ$ from argon vs energy. Y_r has Rutherford scattering energy dependence removed. Plateau between 2.0 and 3.0 Mev corresponds to essentially pure He^{++} beam collected in Faraday cup; increase at lower energies reflects the decrease in the effective charge per particle collected due to admixture of He^+ ions. Results in Table IV are derived from these data.

characteristic energy dependence of Rutherford scattering, and p is proportional to the number of argon atoms per cc. The dashed horizontal line represents the limiting value of Y_r for high energies, where all ions are collected as He^{++} . The departures at the lower energies simply reflect the fact that the average charge per collected particle decreases. Neglecting the He^0 fraction for this energy region [already less than 10% for $E_0 < 500$ kev; see Snitzer²⁷], and defining ρ as the ratio $\text{He}^+/\text{He}^{++}$, we obtain the following expression for N :

$$N = 3.125 \times 10^{12} (2\rho + 1) / (\rho + 1) \quad \text{alphas per microcoulomb.} \quad (\text{A.7})$$

If we define α to be the ratio of Y_r at the plateau to the actual Y_r , we can determine ρ from the simple expression

$$\rho = (1 - \alpha) / (2\alpha - 1). \quad (\text{A.8})$$

In Table IV we list the quantities ρ so obtained. It should be remembered that ρ is also equal to λ^+/λ^{++} , the ratio of the mean free paths for capture and loss of electrons. The energies listed are the energies upon

TABLE IV. Information on charge states of a He beam emerging from nickel foil. E_i = incident beam energy; E_f = energy of the beam emerging from a $445 \mu\text{g}/\text{cm}^2$ nickel foil, estimated from range-energy data in copper; 2α = effective charge per particle collected (see text and Fig. 8).

E_i (Mev)	E_f (Mev)	2α	λ^+/λ^{++}
1.0	0.72	1.23 ± 0.02	1.68 ± 0.15
1.5	0.92	1.77 ± 0.02	0.149 ± 0.013
2.0	1.70	1.00 ± 0.03	0.000 ± 0.015
2.5	2.16	2.02 ± 0.03	-0.010 ± 0.015
2.9	2.58	1.97 ± 0.03	0.015 ± 0.015

emerging from the nickel foil. The fact that the incident beam is singly charged is immaterial, since the rapid exchange of electrons between beam and metal allows the appropriate characteristic equilibrium distribution of charge states to be reached after only a few atomic layers. The values obtained are very rough, especially when the effective charge per particle is nearly two. The quantity 2α represents the effective charge per particle collected. These results go over smoothly into the results of Snitzer²⁷ at lower energies. They generally lie somewhat below the early values found by Rutherford and co-workers for mica.¹ We wish to emphasize, however, that the accuracy of our absolute cross sections in no way depends upon our knowledge of the quantity ρ .

APPENDIX III. PHASE-SHIFT ANALYZER

We have already discussed the determination of the *s*-wave phase shift K_0 at energies where it is the

²⁷ E. Snitzer, Phys. Rev. **89**, 1237 (1953).

only one required to explain the observed angular distributions. Expression (A.1) is not too unwieldy, and can easily be computed for various values of K_0 . However, at 2.5 Mev and 3.0 Mev, we were unable to reproduce the shape of the angular distributions by a single parameter K_0 . In order to allow for two parameters K_0 and K_2 , we built the vectorial nomograph shown in Fig. 9, which was inspired by the vector diagram depicted in Fig. 3(A) of Wheeler's paper on α - α scattering analysis.⁸ The nomograph permits the simple determination of a compromise solution for the (K_0, K_2) pair, taking into account the scattering data at all angles, as well as the experimental uncertainties. The use of the nomograph is limited to the case of a fixed, phase-independent amplitude (Coulomb), plus

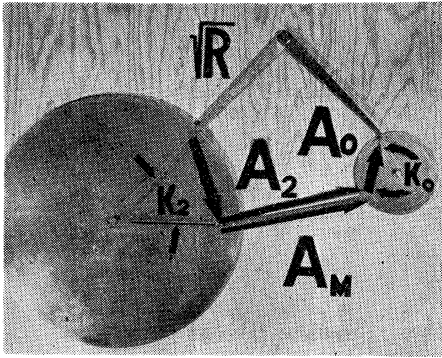


FIG. 9. Mechanical nomograph for phase-shift analysis. Large disk on left represents the d -wave contribution used at a radius A_2 given by Eq. (A.10); at that point the Mott contribution A_M is added vectorially; the small disk to the right represents the s -wave contribution, added vectorially to A_M at a radius A_0 given by Eq. (A.10). The actual scattering amplitude vectors A_2 , A_M , and A_0 are labeled in the diagram; their vector sum \sqrt{R} is shown as the caliper opening and represents the experimental information at a given scattering angle Θ . The Lucite pointers on the two dials sweep out possible pairs of values of K_0 and K_2 , respectively, allowed by the fixed caliper separation \sqrt{R} . Loci of such (K_0, K_2) pairs are shown in Fig. 10, for various scattering angles.

two phase-dependent scattering amplitudes. In our particular case, let us call A_M the Mott scattering amplitude [$=\sqrt{\sigma_M}$, see Eq. (1c)], A_0 the nuclear s -wave amplitude, and A_2 the nuclear d -wave amplitude. Writing Eq. (1a) in the complex amplitude plane for the case including s - and d -wave contributions, we obtain

$$|\sqrt{R}| = \sqrt{(\sigma_M R_2)} = |A_M e^{i\Phi_M} + iA_0 - A_2 e^{2i\xi_2}|, \quad (\text{A.9})$$

where

$$A_0 = A_0(e^{2iK_0} - 1), \quad A_2 = A_2(1 - e^{2iK_2}), \quad (\text{A.10})$$

and

$$\Phi_M = \tan^{-1} \left(\frac{\csc^2 \Theta \sin \alpha + \sec^2 \Theta \sin \beta}{\csc^2 \Theta \cos \alpha + \sec^2 \Theta \cos \beta} \right), \quad (\text{A.11})$$

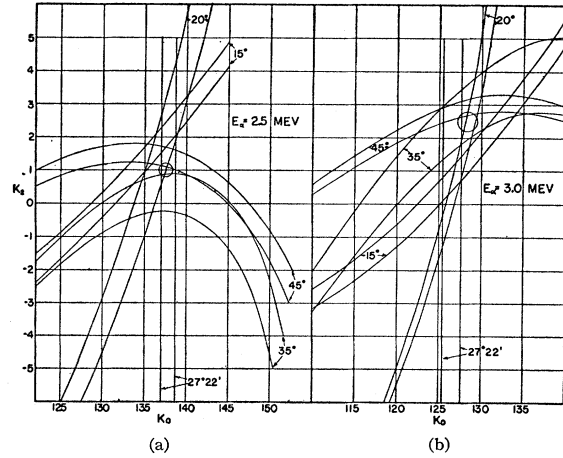


FIG. 10. Phase-shift analysis for α - α scattering when s - and d -wave nuclear interactions contribute in addition to the Coulomb interaction. (a) Analysis of 2.5-Mev data, the lowest energy requiring some d -wave admixture. (b) Analysis of 3.0-Mev data. A given curve represents the locus of possible pairs of K_0 and K_2 compatible with the experimentally found scattering cross section at a given angle and energy, and is obtained from the nomograph shown in Fig. 9 above. The bands of varying widths associated with each angle reflect the experimental uncertainties; the higher-lying limits of each band correspond to the lower bounds of the experimental "ratios to Mott." The vertical bands at $\Theta = 27^\circ 22'$ correspond to the fact that there is no d -wave contribution at this special angle. The unique solutions for K_0 and K_2 are obtained from the intersection of the bands; the small circles indicate the compromise values (with uncertainties) listed in Table II.

and all other quantities have been defined previously. Referring now to the nomograph of Fig. 9, the large dial represents the d wave and is used at a radius $A_2 = 10P_2/\eta$; the small dial represents the s wave and is used at a radius $A_0 = 2/\eta$; the ruler connecting them represents the Mott scattering amplitude A_M . The relative orientations of the three components are determined by the angles Φ_M , i , and $-e^{2i\xi_2}$ for A_M , A_0 , and A_2 , respectively. The dials are marked off in units of $2K_0$ and $2K_2$; it is clear that the Lucite pointers will trace out the phase factors $(e^{2iK_0} - 1)$, etc., and that the black arrows in the figure represent the nuclear s -wave and d -wave amplitudes, respectively. A given "diagram" such as the one illustrated in the figure refers to just one given scattering angle Θ and a given energy. The resultant $\sqrt{R} = \sqrt{(\sigma_M R_2)}$ represents the experimentally known quantity. The procedure is now to adjust a beam compass to the latter distance, and to connect the appropriate points on the two Lucite pointers (corresponding to radii A_0 and A_2 as given above). A certain coupled motion of the two pointers will now be possible, and one reads corresponding pairs of values of K_0 and K_2 . Repeating this procedure with a beam compass opening changed by the experimental uncertainty, we can then plot a K_2 vs K_0 locus, which will be a band containing possible (K_0, K_2) pairs

reproducing one point on an angular distribution curve. This procedure must now be repeated for different scattering angles, i.e. different "diagrams" for each of which we obtain a corresponding band. This process is illustrated in Fig. 10 for 2.5 and 3.0 Mev. The unique solutions for K_0 and K_2 are of course to be found in the areas common to all bands. A special, vertical band obtains at $\Theta=27^\circ 22'$, where $p_2(\cos 2\Theta)$ vanishes, so that only K_0 is determined.

The nomograph is particularly useful for recognizing configurations (scattering angles) of high (or low) sensitivity to experimental error, so that a judicious selection of experimental conditions, insuring minimum uncertainties in K_0 and K_2 , can be made.

APPENDIX IV. GROUND STATE OF Be⁸

We shall evaluate the effect of a narrow s -wave resonance on the scattering of a beam of alpha particles having an effective energy spread $\Delta E = E_2 - E_1$. Our observations, shown in Fig. 5, consist of measurements of the ratio of scattering yield at $\Theta = 45^\circ$ to that at $\Theta = 15^\circ$. We therefore need to average over ΔE the expression plotted in Fig. 6. For $\Theta = 45^\circ$ and an incident energy of 160 kev, Eq. (A.1) becomes

$$R_0(45^\circ) = 1 - a \sin^2 K_0 - b \sin 2K_0, \quad (\text{A.12})$$

where $a=0.419$, $b=0.133$. For simplicity, we shall neglect (1) the variation of $R_0(15^\circ)$ with K_0 , which has a negligible influence, (2) the variation of the "constant" coefficients of $\sin^2 K_0$ and $\sin 2K_0$ with energy through their dependence on η [see Eqs. (1c) and (A.1)], over an energy interval of the order of ΔE , which is very small compared to the resonance energy E_r . We require the average quantity

$$\bar{R}_0(45^\circ) = \frac{1}{\Delta E} \int_{E_1}^{E_2} R_0(45^\circ) dE. \quad (\text{A.13})$$

Substituting the resonant energy dependence of K_0

from Eq. (4) into Eq. (A.11), we obtain after integration

$$\begin{aligned} \bar{R}_0(45^\circ) = 1 - \frac{a\Gamma}{2\Delta E} & \left[\tan^{-1} \left(\frac{2(E_r - E_1)}{\Gamma} \right) \right. \\ & \left. + \tan^{-1} \left(\frac{2(E_2 - E_r)}{\Gamma} \right) \right] \\ & - \frac{b\Gamma}{2\Delta E} \ln \left[\frac{(E_r - E_1)^2 + (\Gamma/2)^2}{(E_2 - E_r)^2 + (\Gamma/2)^2} \right]. \quad (\text{A.14}) \end{aligned}$$

Let us assume first that the energy spread ΔE straddles the resonance energy E_r , i.e., that $E_r - E_1 = E_2 - E_r = \Delta E/2$. The last term of (A.13) then vanishes, and if we call δ the departure from unity, we have

$$\delta = \frac{a\Gamma}{\Delta E} \tan^{-1} \left(\frac{\Delta E}{\Gamma} \right) \cong \frac{\pi a\Gamma}{2\Delta E}, \quad (\text{A.15})$$

since $\Delta E \gg \Gamma$. Another, but probably less realistic way of estimating the effect, is to let $E_2 = E_r$, which will evidently maximize δ , as can be seen from Fig. 6. We then obtain from (A.13), since $E_r - E_1 = \Delta E$,

$$\delta \cong \frac{\pi a\Gamma}{4\Delta E} + \frac{b\Gamma}{\Delta E} \ln \left(\frac{2\Delta E}{\Gamma} \right). \quad (\text{A.16})$$

Using the numerical values for a and b , taking $\Delta E = 250$ ev, and requiring δ and δ' to be less than 0.02, i.e., assuming that we could have detected a 2% departure from the average trend shown in Fig. 5, we obtain

$$\Gamma \leq 7 \text{ ev}; \quad \Gamma' \leq 4 \text{ ev}.$$

To be conservative, we shall use the larger value Γ as our absolute lower limit. The limit on the actual level width for Be⁸ will then be

$$\Gamma_0 \leq 3.5 \text{ ev}.$$

Further inferences to be made from this limit are discussed in Sec. IV(b).

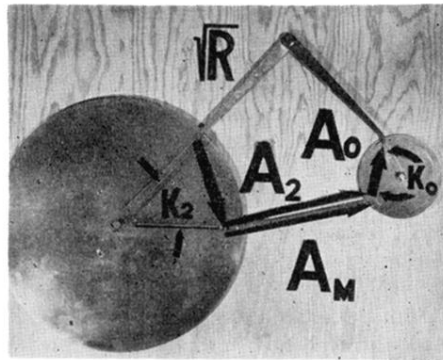


FIG. 9. Mechanical nomograph for phase-shift analysis. Large disk on left represents the d -wave contribution used at a radius A_2 given by Eq. (A.10); at that point the Mott contribution A_M is added vectorially; the small disk to the right represents the s -wave contribution, added vectorially to A_M at a radius A_0 given by Eq. (A.10). The actual scattering amplitude vectors A_2 , A_M , and A_0 are labeled in the diagram; their vector sum \sqrt{R} is shown as the caliper opening and represents the experimental information at a given scattering angle Θ . The Lucite pointers on the two dials sweep out possible pairs of values of K_0 and K_2 , respectively, allowed by the fixed caliper separation \sqrt{R} . Loci of such (K_0, K_2) pairs are shown in Fig. 10, for various scattering angles.